

# Study of $e^+e^- \rightarrow \eta\phi$ via Initial State Radiation at Belle

The Belle Collaboration

(Dated: September 5, 2022)

## Abstract

Using  $980 \text{ fb}^{-1}$  of data collected on and around the  $\Upsilon(nS)$  ( $n = 1, 2, 3, 4, 5$ ) resonances with the Belle detector at the KEKB collider, we measure the cross section of  $e^+e^- \rightarrow \eta\phi$  from threshold to 3.95 GeV via initial-state radiation. From a multi-parameter fit assuming  $\phi(2170)$  exists in the  $\eta\phi$  final state according to previous measurement by BESIII, the resonant parameters of  $\phi(1680)$  are determined to be  $m_{\phi(1680)} = (1683 \pm 7 \pm 9) \text{ MeV}/c^2$  (statistical and systematic errors, respectively),  $\Gamma_{\phi(1680)} = (149 \pm 12 \pm 13) \text{ MeV}$  and, depending on the possible presence of interfering resonances,  $\Gamma_{\phi(1680)}^{e^+e^-} \cdot \mathcal{B}[\phi(1680) \rightarrow \eta\phi] = (122 \pm 6 \pm 13) \text{ eV}$ ,  $(219 \pm 15 \pm 18) \text{ eV}$ ,  $(163 \pm 11 \pm 13) \text{ eV}$  or  $(203 \pm 12 \pm 18) \text{ eV}$ . The branching fraction of  $\phi(1680) \rightarrow \eta\phi$  decay is determined to be approximately 20%. Additionally, the branching fraction for  $J/\psi \rightarrow \eta\phi$  is measured to be  $(7.1 \pm 1.0 \pm 0.5) \times 10^{-4}$ . However, there is no significant observed  $\phi(2170)$  signal in the  $\eta\phi$  final states in this analysis, and correspondingly the upper limit for  $\Gamma_{\phi(2170)}^{e^+e^-} \cdot \mathcal{B}(\phi(2170) \rightarrow \eta\phi)$  is determined to be either 0.17 eV (for two fits), or 18.6 eV (remaining two fits), at 90% confidence level.

PACS numbers: 14.40.Gx, 13.25.Gv, 13.66.Bc

## I. INTRODUCTION

Quarkonium and quarkonium-like states play an important role in understanding Quantum Chromodynamics (QCD), which is the generally accepted theory for strong interactions between quarks and gluons. However, there are no first-principles methods to derive the spectrum and properties of hadrons from the QCD Lagrangian. Alternatively, the more phenomenological Quark Model is used comprehensively [1]. Although hadrons with multiple quarks ( $n > 3$ ), with only gluons, or with bound hadrons, etc., are allowed according to QCD, only recently have accordant candidates been identified. Since the discovery of  $X(3872)$  in 2003 by the Belle experiment [2], dozens of new states have been observed by Belle, BaBar, BESIII, CLEO, LHCb, etc. However, these new states do not easily fit into the hadronic spectrum derived from the Quark Model, indicating that new types of hadrons may have already been observed. For example, the charged charmonium-like states, such as  $Z_c(3900)$  [3],  $X(4020)^\pm$  [4] and  $X(4055)^\pm$  [5], are generally interpreted as exotic states.

Hadronic transitions have contributed significantly to the discoveries of quarkonium(-like) states, such as the  $Y(4260)$  in  $e^+e^- \rightarrow \pi^+\pi^- J/\psi$  via initial-state radiation (ISR) by the BaBar experiment [6]. In searching for an  $s\bar{s}$  version of the  $Y(4260)$ , the  $Y(2175)$  (now called ‘ $\phi(2170)$ ’) was discovered in  $e^+e^- \rightarrow \pi^+\pi^-\phi$  via ISR by BaBar [7], and later confirmed by Belle [8]. There are several interpretations of the  $\phi(2170)$ , such as a regular  $s\bar{s}$  meson [9, 10], an  $s\bar{s}g$  hybrid [11], a tetraquark state [12–14], a  $\Lambda\bar{\Lambda}$  bound state [15–18], an  $S$ -wave threshold effect [19], or a three-meson system  $\phi K\bar{K}$  [20]. In a recent lattice QCD calculation [21], the properties of the lowest two states comply with those of  $\phi(1020)$  and  $\phi(1680)$ , but with no obvious correspondence to the  $\phi(2170)$ . In searching for  $\phi(2170)$  in other hadronic transitions, BaBar studied the  $e^+e^- \rightarrow \eta\phi$  process via ISR using a  $232 \text{ fb}^{-1}$  data sample and found several hundreds of  $\eta\phi$  signal events, among which hints of an excess were observed around  $2.1 \text{ GeV}/c^2$  [22]. Assuming these hints correspond to bound  $\phi''$  state, BaBar estimated the mass  $M_{\phi''} = (2125 \pm 22 \pm 10) \text{ MeV}/c^2$ , width  $\Gamma_{\phi''} = (61 \pm 50 \pm 13) \text{ MeV}$  and product of the partial width times branching fraction  $\Gamma_{\phi''}^{e^+e^-} \mathcal{B}(\phi'' \rightarrow \phi\eta) = (1.7 \pm 0.7 \pm 1.3) \text{ eV}$ . (Hereinafter, quoted uncertainties are statistical systematic, respectively.) The CMD-3 experiment measured the process  $e^+e^- \rightarrow K\bar{K}\eta$  from 1.59 to 2.007 GeV and found it is dominated by the  $\eta\phi$  contribution, and then calculated the contribution to the anomalous magnetic moment of muon:  $\alpha_\mu^{\eta\phi}(E < 1.8 \text{ GeV}) = (0.321 \pm 0.015 \pm 0.016) \times 10^{-10}$ ,  $\alpha_\mu^{\eta\phi}(E < 2.0 \text{ GeV}) = (0.440 \pm 0.015 \pm 0.022) \times 10^{-10}$  [23]. Recently, BESIII measured  $e^+e^- \rightarrow \phi\eta'$  with a data sample taken at center of mass (CM) energies ( $\sqrt{s}$ ) ranging from 2.05 to 3.08 GeV and observed a resonance near 2.17 GeV with a statistical significance exceeding  $10\sigma$  [24]. If both of these correspond to decays of the  $\phi(2170)$ , one could infer the ratio  $\mathcal{B}(\phi(2170) \rightarrow \phi\eta)/\mathcal{B}(\phi(2170) \rightarrow \phi\eta') = 0.23 \pm 0.10 \pm 0.18$ , which is smaller than the prediction of  $s\bar{s}g$  hybrid models by several orders of magnitude. However, due to limited statistics, the uncertainty in  $\Gamma_{\phi''}^{e^+e^-} \mathcal{B}(\phi'' \rightarrow \phi\eta)$  from BaBar is large. BESIII also measured the Born cross section of  $e^+e^- \rightarrow \eta\phi$  and determined the  $\phi(2170)$  parameters to be  $m_{\phi(2170)} = (2163.5 \pm 6.2 \pm 3.0) \text{ MeV}/c^2$ ,  $\Gamma_{\phi(2170)} = (31.1^{+21.1}_{-11.6} \pm 1.1) \text{ MeV}$ , and  $\Gamma_{\phi(2170)}^{e^+e^-} \mathcal{B}(\phi(2170) \rightarrow \phi\eta) = (0.24^{+0.12}_{-0.07}) \text{ eV}$  or  $(10.11^{+3.87}_{-3.13}) \text{ eV}$  [25]. The signal significance of  $\phi(2170)$  is determined to be  $6.9\sigma$ . In that analysis, BESIII used, as input, the cross section of  $e^+e^- \rightarrow \eta\phi$  below 2.0 GeV (dominated by the  $\phi(1680)$  signal) measured by BaBar [22] in the determination of the  $\phi(2170)$  resonant parameters.

In this article, we report a study of the  $e^+e^- \rightarrow \eta\phi$  process via ISR with the Belle detector

[26] at the KEKB asymmetric-energy  $e^+e^-$  collider [27]. The integrated luminosity used in this analysis is  $980 \text{ fb}^{-1}$ , of which  $\sim 70\%$  were collected at the  $\Upsilon(4S)$  resonance, with the remainder accumulated either at the other  $\Upsilon(nS)$  ( $n = 1, 2, 3, 5$ ) resonances or at  $\sqrt{s}$  lower than the  $\Upsilon$  resonances by tens of MeV. This data sample is much larger than the one used in the previous analysis [22]. We scan the  $\phi(1680) \rightarrow \eta\phi$  final state over the energy interval from  $1.7 \text{ GeV}/c^2$  to  $3.95 \text{ GeV}/c^2$ , which also covers the signal regions for  $\phi(2170)$  and  $J/\psi$ . The well improved precision of the cross section of  $e^+e^- \rightarrow \eta\phi$  will be helpful to calculate the  $\alpha_\mu^{\eta\phi}$  [28]. The  $\phi$  is reconstructed from its decay to  $K^+K^-$  final state, and the  $\eta$  is reconstructed from its decay to either the  $\gamma\gamma$  or  $\pi^+\pi^-\pi^0$  final states.

## II. THE BELLE DETECTOR AND MONTE CARLO (MC) SIMULATION

The Belle detector is a large-solid-angle magnetic spectrometer consisting of a silicon vertex detector, a 50-layer central drift chamber, an array of aerogel threshold Cherenkov counters, a barrel-like arrangement of time-of-flight scintillation counters, and an electromagnetic calorimeter (ECL) comprised of CsI(Tl) crystals located inside a superconducting solenoid coil that provides a 1.5T magnetic field. An iron flux return located outside of the coil is instrumented to detect  $K_L^0$  mesons and to also identify muons. With the origin of the coordinate system defined as the nominal interaction point, the  $z$  axis is aligned with the direction opposite the  $e^+$  beam and is parallel to the direction of the magnetic field within the solenoid. The  $y$  axis is vertical upward, and the  $x$  axis is horizontal and completes the right-handed coordinate frame. The polar angle  $\theta$  and azimuthal angle  $\phi$  are measured relative to the positive  $z$  and  $x$  axes, respectively.

The PHOKHARA event generator [29] is used to simulate the process  $e^+e^- \rightarrow \eta\phi$  via ISR for optimization of selection criteria and the efficiency estimation. One or more ISR photons ( $\gamma_{\text{ISR}}$ ) are emitted before forming a resonance  $Y$ , which then decays to  $\eta\phi$  with  $\phi \rightarrow K^+K^-$  and  $\eta \rightarrow \pi^+\pi^-\pi^0$  or  $\gamma\gamma$ . In the generator, the resonance  $Y$  could be  $\phi(1680)$ ,  $\phi(2170)$ ,  $J/\psi$  or a particle with mass fixed to a value between 1.6 and 4.0  $\text{GeV}/c^2$  and width fixed to zero. Since the  $\phi(1680)$  dominates the  $\eta\phi$  final states, we use the MC sample of  $\phi(1680)$  as the nominal signal MC sample. A GEANT3-based MC simulation [30] is used to simulate the Belle detector response.

## III. EVENT SELECTION CRITERIA

To study the  $\eta\phi$  final states, a  $\phi$  candidate is reconstructed from a  $K^+K^-$  pair and an  $\eta$  candidate is reconstructed in either the  $\gamma\gamma$  or  $\pi^+\pi^-\pi^0$  ( $\pi^0 \rightarrow \gamma\gamma$ ) modes. Hereinafter, the reconstruction channel with  $\eta \rightarrow \gamma\gamma$  is called the “ $\gamma\gamma$  mode”, and the three-pion mode is referred to as the “ $\pi^+\pi^-\pi^0$  mode.” For a candidate event, we require two (four) well-measured charged tracks with zero net charge for the  $\gamma\gamma$  ( $\pi^+\pi^-\pi^0$ ) mode. A well-measured charged track is defined as one having impact parameters with respect to the interaction point satisfying  $dr < 1.5 \text{ cm}$  in the  $r-\phi$  plane and  $|dz| < 5 \text{ cm}$  in the  $r-z$  plane, respectively. For each charged track, information from different detector subsystems is combined to form a likelihood  $\mathcal{L}_i$  for each putative particle species ( $i$ ) [31]. Tracks with  $\mathcal{R}_K = \frac{\mathcal{L}_K}{\mathcal{L}_K + \mathcal{L}_\pi} > 0.6$  are identified as kaons, while those with  $\mathcal{R}_K < 0.4$  are identified as pions, with an efficiency of about 95% for  $K - \pi$  separation.

Each photon candidate is a cluster in the ECL that is unmatched to the extrapolated

trajectories of any charged tracks. The photon with the highest energy is identified to be  $\gamma_{\text{ISR}}$ . In the reconstruction of  $\pi^0$  candidates, the energy of a photon candidate is required to have  $E_\gamma > 25$  MeV in the barrel ( $\cos\theta \in [-0.63, 0.85]$ ) and  $E_\gamma > 50$  MeV in the endcaps ( $\cos\theta \in [-0.91, -0.65] \cup [0.85, 0.98]$ ). The  $M_{\gamma\gamma}$  mass resolution is about 6 MeV/ $c^2$ , and the signal region of the  $\pi^0$  is defined to be  $120 < M_{\gamma\gamma} < 150$  MeV/ $c^2$  with  $\chi^2(\pi^0) < 25$  (the  $\chi^2$  value returned for the mass fit to each  $\pi^0$  candidate). Events with  $\gamma \rightarrow e^+e^-$  conversions are removed by requiring  $\mathcal{R}_e < 0.75$  for the  $\pi^+\pi^-$  tracks from  $\eta$  decays. In this case, the particle identification variable for electron/positron in conversion products is defined as  $\mathcal{R}_e \equiv \mathcal{L}_e/(\mathcal{L}_e + \mathcal{L}_{\text{hadrons}})$ . In the reconstruction of  $\eta \rightarrow \gamma\gamma$ , two photon candidates are required, each with energy satisfying  $E_{\gamma_l} > 120$  MeV and  $E_{\gamma_h} > 350$  MeV, where the subscript  $l$  ( $h$ ) signifies the lower (higher) energy photon in the laboratory system. The efficiency of the energy requirement is  $(96.6 \pm 0.1)\%$  (statistical error only), as determined from signal MC simulation.

The scatter plots displaying the dikaon ( $M_{K^+K^-}$ ) invariant mass versus the  $\pi^+\pi^-\pi^0$  invariant mass ( $M_{\pi^+\pi^-\pi^0}$ ), or the  $\gamma_l\gamma_h$  invariant mass ( $M_{\gamma\gamma}$ ) are shown in Fig. 1. A  $K^+K^-$  pair is treated as a  $\phi$  candidate if  $|M_{K^+K^-} - m_\phi| < 12$  MeV/ $c^2$  (the mass resolution is  $\sim 4$  MeV/ $c^2$ ), where  $m_\phi$  is the  $\phi$  nominal mass [32]. This mass interval requirement for the  $\phi$  retains  $(97.1 \pm 0.6)\%$  of  $\phi$  candidates in data and  $(97.4 \pm 0.1)\%$  in the signal MC simulation, respectively. The lower and upper  $\phi$  mass sidebands are defined to be  $0.990 < M_{K^+K^-} < 1.002$  GeV/ $c^2$  and  $1.036 < M_{K^+K^-} < 1.048$  GeV/ $c^2$ . A fit to the  $M_{\pi^+\pi^-\pi^0}$  or  $M_{\gamma\gamma}$  distribution with a Gaussian function for the  $\eta$  signal, and a smooth second-order polynomial function for background yields a mass resolution of  $\sigma_{\pi^+\pi^-\pi^0} = 4.2$  MeV/ $c^2$  in the  $\pi^+\pi^-\pi^0$  mode and  $\sigma_{\gamma\gamma} = 11.3$  MeV/ $c^2$  in the  $\gamma\gamma$  mode. We define the  $\eta$  signal mass interval by  $|M_{\pi^+\pi^-\pi^0/\gamma\gamma} - m_\eta| < 3\sigma_{\pi^+\pi^-\pi^0/\gamma\gamma}$ , and the sideband regions are defined by  $|M_{\pi^+\pi^-\pi^0} - m_\eta \pm 9\sigma_{\pi^+\pi^-\pi^0/\gamma\gamma}| < 3\sigma_{\pi^+\pi^-\pi^0/\gamma\gamma}$ , where  $m_\eta$  is the nominal  $\eta$  mass [32]. The central (surrounding) rectangles of Fig. 1 show the  $\eta\phi$  signal (sideband) regions. With  $S1$ ,  $S2$  and  $S3$  representing the sum of the events in the two adjacent horizontal ( $S1$ ) and vertical ( $S2$ ) sideband boxes, and ( $S3$ ) the four diagonal sideband boxes relative to the signal box, the normalization of the two-dimensional (2D) sidebands is given by  $S = a \cdot S1 + b \cdot S2 - ab \cdot S3$ , where  $a = 0.84 \pm 0.05$  and  $b = 0.52 \pm 0.03$  are the appropriate areal scale factors, according to the  $M_{K^+K^-}$  and  $M_{\pi^+\pi^-\pi^0/\gamma\gamma}$  distributions. These 2D sidebands are used to estimate the background level in the  $\eta\phi$  signal region.

For most of the ISR events, the missing mass squared of the reconstructed  $\eta$ ,  $\phi$ , and  $\gamma_{\text{ISR}}$  candidates ( $M_{\text{miss}}^2(\gamma_{\text{ISR}}\eta\phi)$ ) is close to zero, consistent with either complete reconstruction or a low-energy, second ISR photon eluding detection (Fig. 2(a)). We also require  $|M_{\text{miss}}^2(\gamma_{\text{ISR}}\eta\phi)| < 0.1$  GeV $^2/c^4$  with a mass-selection efficiency of  $(97.7 \pm 0.3)\%$  in the  $\pi^+\pi^-\pi^0$  mode and  $(97.1 \pm 0.3)\%$  in the  $\gamma\gamma$  mode. Figures 2(b) and (c) illustrate the good agreement between data and signal MC simulations for the distributions of visible energy of all final state photons and charged particles ( $E_{\text{vis}}$ ), as well as the polar angle of the  $\eta\phi$  system in the  $e^+e^-$  CM frame ( $\cos\theta(\eta\phi)$ ), confirming that the signal events are produced via ISR.

#### IV. INVARIANT MASS SPECTRUM OF $\eta\phi$ FROM ISR PRODUCTION

After imposing the selection criteria, the distributions of the  $\eta\phi$  invariant mass ( $M_{\eta\phi}$ ) from the two modes are shown in Fig. 3, together with the backgrounds estimated from the scaled 2D sidebands. Using  $M_{\eta\phi} \equiv M_{\pi^+\pi^-\pi^0 K^+K^-} - M_{\pi^+\pi^-\pi^0} - M_{K^+K^-} + m_\eta + m_\phi$  for the  $\eta \rightarrow \pi^+\pi^-\pi^0$  mode and  $M_{\eta\phi} \equiv M_{\gamma\gamma K^+K^-} - M_{\gamma\gamma} - M_{K^+K^-} + m_\eta + m_\phi$  for the  $\eta \rightarrow \gamma\gamma$  mode,

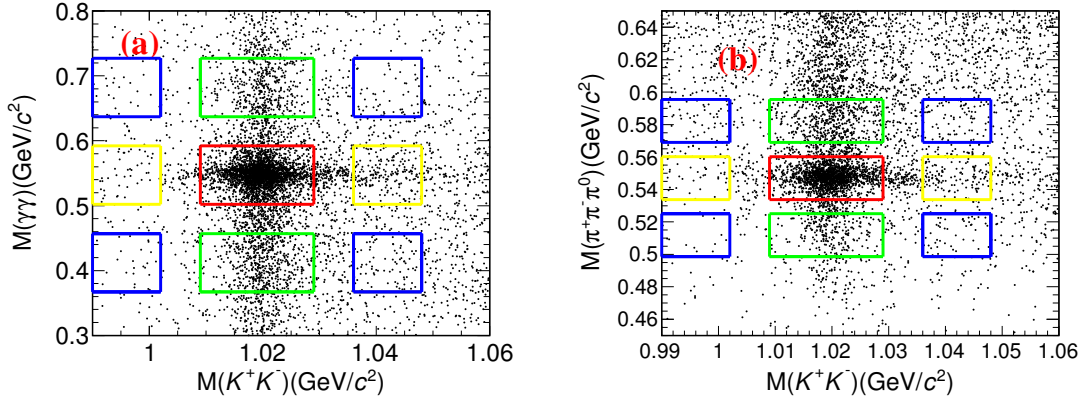


FIG. 1. Invariant mass distributions of (a)  $K^+K^-$  versus  $\gamma\gamma$  and (b)  $K^+K^-$  versus  $\pi^+\pi^-\pi^0$  for the selected  $\pi^+\pi^-\pi^0 K^+K^-$  or  $\gamma\gamma K^+K^-$  candidates having  $\eta\phi$  invariant mass below  $3.5 \text{ GeV}/c^2$ . The box in the center of each plot shows the  $\eta\phi$  signal region, while the surrounding boxes show the sideband regions, defined according to the scheme described in the text.

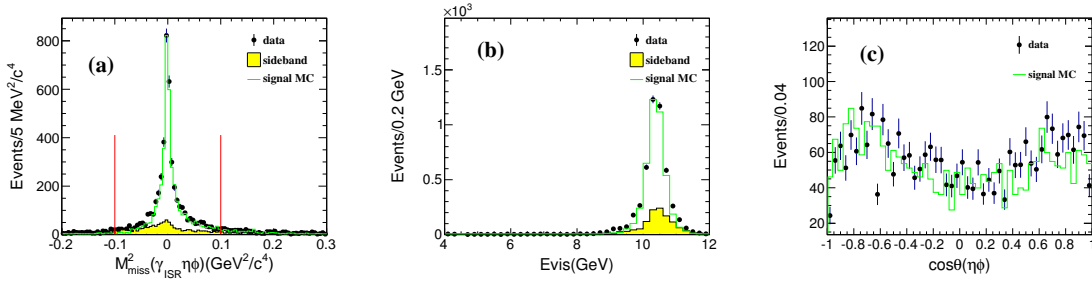


FIG. 2. The ISR characteristics of the final states. Plot (a) shows the missing mass squared of  $\eta\phi$  and  $\gamma_{\text{ISR}}$ , (b) shows the visible energy in the detector and (c) shows the angular distribution of  $\eta\phi$  in the  $e^+e^-$  CM frame. The dots with error bars correspond to data while the shaded histograms correspond to backgrounds estimated from the 2D sidebands. The unshaded histograms are the signal MC simulations. In plot (c), the backgrounds estimated from 2D sidebands have been subtracted from the data.

the mass resolution of  $\eta\phi$  is about  $6 \text{ MeV}/c^2$ . The number of obtained  $\eta\phi$  signal events is about seven times larger than the previous work [22], although there is not an obvious  $\phi''$  signal.

There are clear  $J/\psi$  signals in both the  $\pi^+\pi^-\pi^0$  mode and the  $\gamma\gamma$  mode. Performing an unbinned maximum likelihood fit to the combined  $M_{\eta\phi}$  spectrum of the two modes, with a Gaussian function for the  $J/\psi$  signals and a second-order polynomial function for the backgrounds. The  $J/\psi$  signal yield is  $N_{\text{sig}}^{\text{fit}} = (99 \pm 14)$ . To estimate the fitting systematic error, polynomial functions of either first- or third-order are also used for the background parameterization. The branching fraction for the  $J/\psi \rightarrow \eta\phi$  decay is calculated using

$$\mathcal{B}(J/\psi \rightarrow \eta\phi) = \frac{N_{\text{sig}}^{\text{fit}}}{\sigma_{\text{ISR}}^{\text{prod}} \times \mathcal{L} \times \varepsilon \times \mathcal{B}(\phi \rightarrow K^+K^-) \times \mathcal{B}(\eta \rightarrow \gamma\gamma/\pi^+\pi^-\pi^0)}, \quad (1)$$

where  $\mathcal{L}$ ,  $\varepsilon$ ,  $\mathcal{B}(\phi \rightarrow K^+K^-)$ ,  $\mathcal{B}(\eta \rightarrow \gamma\gamma/\pi^+\pi^-\pi^0)$  are the integrated luminosity of the Belle

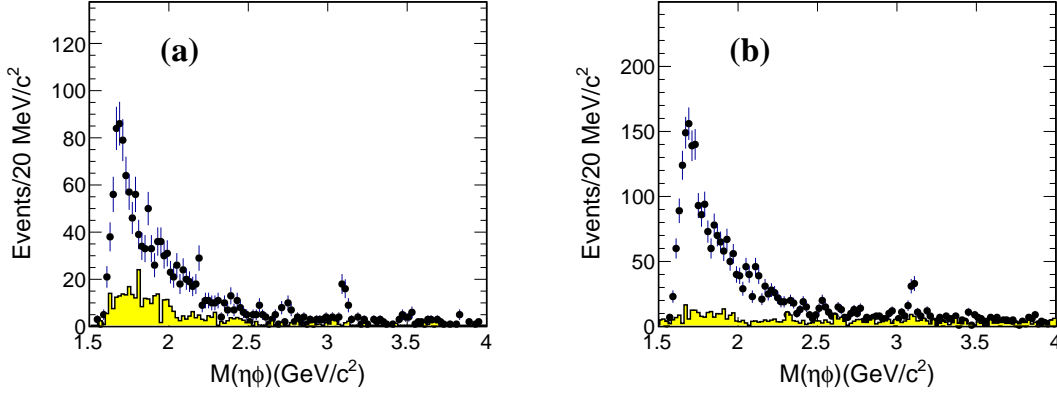


FIG. 3. Invariant mass  $\eta\phi$  distributions in (a) the  $\pi^+\pi^-\pi^0$  mode and (b) the  $\gamma\gamma$  mode from data. The points with error bars are from the signal region and the shaded histograms are backgrounds estimated from the 2D sidebands.

data sample, the detection efficiency, the  $\phi \rightarrow K^+K^-$  branching fraction, and the combined branching fraction for the  $\eta \rightarrow \gamma\gamma$  and  $\pi^+\pi^-\pi^0$  final states [32], respectively;  $\sigma_{\text{ISR}}^{\text{prod}}(J/\psi) = 37.5$  pb is the cross section for  $J/\psi$  production via ISR for the Belle experiment [8]. With systematic uncertainties as described below in Sec. VI, the branching fraction of  $J/\psi \rightarrow \eta\phi$  is measured to be  $(7.1 \pm 1.0 \pm 0.5) \times 10^{-4}$ , which agrees well with the world average value of  $(7.4 \pm 0.8) \times 10^{-4}$  [32].

We observe a clear  $\phi(1680)$  signal in the  $\eta\phi$  final state. However, the  $\phi(2170)$  is not as prominent as in the previous BESIII [25] analysis. An unbinned maximum likelihood fit is performed to the  $M_{\eta\phi}$  mass spectra  $\in [1.55, 2.85]$   $\text{GeV}/c^2$  using signal candidate events and 2D sideband events, simultaneously. Similar to the parametrization in BaBar's measurement [22], the parametrization for the cross section of  $e^+e^- \rightarrow \eta\phi$  at  $\sqrt{s}$  takes the form

$$\sigma_{\eta\phi}(\sqrt{s}) = 12\pi \mathcal{P}_{\eta\phi}(\sqrt{s}) |A_{\eta\phi}^{n.r.}(\sqrt{s}) + A_{\eta\phi}^{\phi(1680)}(\sqrt{s}) + A_{\eta\phi}^{\phi(2170)}(\sqrt{s})|^2, \quad (2)$$

where  $\mathcal{P}_{\eta\phi}$  is the phase space of the final state,  $A_{\eta\phi}^{n.r.}(\sqrt{s}) = a_0/s^{a_1}$  describes the non-resonant contribution (mainly due to the tails of resonances below threshold), and  $A_{\eta\phi}^{\phi(1680)}$  ( $A_{\eta\phi}^{\phi(2170)}$ ) is the  $\phi(1680)$  ( $\phi(2170)$ ) amplitude. The  $\phi(1680)$  resonance amplitude is described by a Breit-Wigner (BW) function

$$A_{\eta\phi}^{\phi(1680)}(\sqrt{s}) = \sqrt{\mathcal{B}_{\phi(1680)}^{\eta\phi} \Gamma_{\phi(1680)}^{e^+e^-}} \frac{\sqrt{\Gamma_{\phi(1680)}/\mathcal{P}_{\eta\phi}(M_{\phi(1680)}^2)} e^{i\theta_{\phi(1680)}}}{M_{\phi(1680)}^2 - s - i\sqrt{s}\Gamma_{\phi(1680)}(\sqrt{s})}, \quad (3)$$

where  $M_{\phi(1680)}$ ,  $\Gamma_{\phi(1680)}$  and  $\Gamma_{\phi(1680)}^{e^+e^-}$  are the mass, the total width and the partial width to  $e^+e^-$  for the  $\phi(1680)$ , respectively.  $\mathcal{B}_{\phi(1680)}^{\eta\phi}$  is the branching fraction for  $\phi(1680) \rightarrow \eta\phi$  and  $\theta_{\phi(1680)}$  is the relative phase. As shown in BaBar's measurement [22], several major decays of  $\phi(1680)$  contribute to  $\Gamma_{\phi(1680)}$ , such as  $KK^*(892)$  and  $\eta\phi$ . Since  $\mathcal{B}_{\phi(1680)}^{KK^*(892)} \approx 2 \times \mathcal{B}_{\phi(1680)}^{\eta\phi}$ , the phase space effect of  $KK^*(892)$  can not be ignored in describing  $\Gamma_{\phi(1680)}$ . Therefore, we take the form as in Ref [22]:

$$\Gamma_{\phi(1680)}(\sqrt{s}) = \Gamma_{\phi(1680)} \left[ \frac{\mathcal{P}_{KK^*(892)}(\sqrt{s})}{\mathcal{P}_{KK^*(892)}(M_{\phi(1680)})} \mathcal{B}_{\phi(1680)}^{KK^*(892)} + \frac{\mathcal{P}_{\eta\phi}(\sqrt{s})}{\mathcal{P}_{\eta\phi}(M_{\phi(1680)})} \mathcal{B}_{\phi(1680)}^{\eta\phi} \right]$$

$$+(1 - \mathcal{B}_{\phi(1680)}^{\eta\phi} - \mathcal{B}_{\phi(1680)}^{KK^*(892)})]. \quad (4)$$

Here,  $\mathcal{P}_{KK^*(892)}$  is the phase space of the  $\phi(1680) \rightarrow KK^*(892)$  decay. The other decays of  $\phi(1680)$  are neglected, and their phase space dependence correspondingly ignored. Since both the  $KK^*(892)$  and the  $\eta\phi$  contain a vector meson ( $V$ ) and a pseudoscalar meson ( $P$ ), the phase takes the form

$$\mathcal{P}_{VP}(\sqrt{s}) = \left[ \frac{(s + M_V^2 - M_P^2)^2 - 4M_V^2 s}{s} \right]^{3/2}. \quad (5)$$

Since there is no measurement of the  $KK^*(892)$  final state in this work, we take  $\mathcal{B}_{\phi(1680)}^{\eta\phi}/\mathcal{B}_{\phi(1680)}^{KK^*(892)}$  directly from Ref. [22].

The  $A_{\eta\phi}^{\phi(2170)}$  is described by

$$A_{\eta\phi}^{\phi(2170)}(s) = \sqrt{\mathcal{B}_{\phi(2170)}^{\eta\phi} \Gamma_{\phi(2170)}^{e^+e^-}} \frac{\sqrt{\Gamma_{\phi(2170)}/\mathcal{P}_{\eta\phi}(M_{\phi(2170)}^2)} e^{i\theta_{\phi(2170)}}}{M_{\phi(2170)}^2 - s - i\sqrt{s}\Gamma_{\phi(2170)}} \cdot \frac{B(p)}{B(p')}, \quad (6)$$

where  $B(p)$  is the  $P$ -wave Blatt-Weisskopf form factor and  $p$  ( $p'$ ) is the breakup momentum corresponding to the  $\sqrt{s}$  ( $M_{\phi(2170)}$ ).

The efficiencies of the  $M_{\eta\phi}$  signal selection are determined from MC samples generated in the range  $1.65 < M_{\eta\phi} < 2.8$  GeV/ $c^2$ , and are found to be roughly constant (1.35%) over this mass interval. The effective integrated luminosity of ISR is calculated according to the theoretical prescription from [33], corresponding to 45 pb $^{-1}$  per 10 MeV near 1.65 GeV and increasing to about 80 pb $^{-1}$  per 10 MeV near 4.0 GeV. The 2D sideband events from  $S_1$ ,  $S_2$  and  $S_3$  are described by three Landau functions; exponential functions are considered to estimate the systematic uncertainty.

Assuming the existence of  $\phi(2170)$  in the  $\eta\phi$  final state, and fitting using the mass and width of  $\phi(2170)$  reported by BESIII [25], there are four solutions of equivalent quality, having the same  $M_{\phi(1680)}$  and  $\Gamma_{\phi(1680)}$ . The fit results are shown in Fig. 4 and Table I. The reduced chi-squared of the fit to the  $M_{\eta\phi}$  spectrum is  $\chi^2/ndf = 77/56$ . The  $\phi(1680)$  resonant parameters are determined to be  $M_{\phi(1680)} = (1683 \pm 7 \pm 9)$  MeV/ $c^2$ ,  $\Gamma_{\phi(1680)} = (149 \pm 12 \pm 13)$  MeV, and  $\mathcal{B}_{\phi(1680)}^{\eta\phi} \Gamma_{\phi(1680)}^{e^+e^-} = (122 \pm 6 \pm 13)$  eV,  $(219 \pm 15 \pm 18)$  eV,  $(163 \pm 11 \pm 13)$  eV or  $(203 \pm 12 \pm 18)$  eV for the four solutions. The branching fraction  $\mathcal{B}_{\phi(1680)}^{\eta\phi}$  obtained from the fit is  $(18 \pm 2 \pm 1)\%$ ,  $(19 \pm 4 \pm 2)\%$ ,  $(21 \pm 2 \pm 1)\%$  or  $(17 \pm 4 \pm 2)\%$  for the four solutions. The statistical significance of  $\phi(2170)$  is determined to be  $1.7\sigma$  by comparing the value of  $\Delta(-2\ln\mathcal{L}) = -2\ln(\mathcal{L}_{\max}/\mathcal{L}_0)$  and the change in the number of free parameters in the fits, where  $\mathcal{L}_{\max}$  is the likelihood with  $\phi(2170)$  and  $\mathcal{L}_0$  without  $\phi(2170)$ . The quantity  $\mathcal{B}_{\phi(2170)}^{\eta\phi} \Gamma_{\phi(2170)}^{e^+e^-}$  is determined to be  $(0.09 \pm 0.05)$  eV,  $(0.06 \pm 0.02)$  eV,  $(16.7 \pm 1.2)$  eV or  $(17.0 \pm 1.2)$  eV in the four solutions. The upper limit for  $\phi(2170)$  production at 90% confidence level (C.L.) is determined by integrating the likelihood versus the  $\phi(2170)$  yield, with the upper limit degraded by a factor of  $1/(1 - \sigma_{\text{sys}})$  to account for systematic uncertainties. (The systematic uncertainties in the fit results and  $\sigma_{\text{sys}}$  are described below in Sec. VI.) Finally, the upper limits for  $\mathcal{B}_{\phi(2170)}^{\eta\phi} \Gamma_{\phi(2170)}^{e^+e^-}$  are determined to be 0.17 eV (Solutions I and II), or 18.6 eV (Solutions III and IV) at 90% confidence level, respectively. Since the  $\phi(2170)$  is not significant in our measurement, another fit without  $\phi(2170)$  in Eq. 2 is performed, as also indicated in Table I. There is no obvious difference in quality between the curves from fits with or without  $\phi(2170)$ .

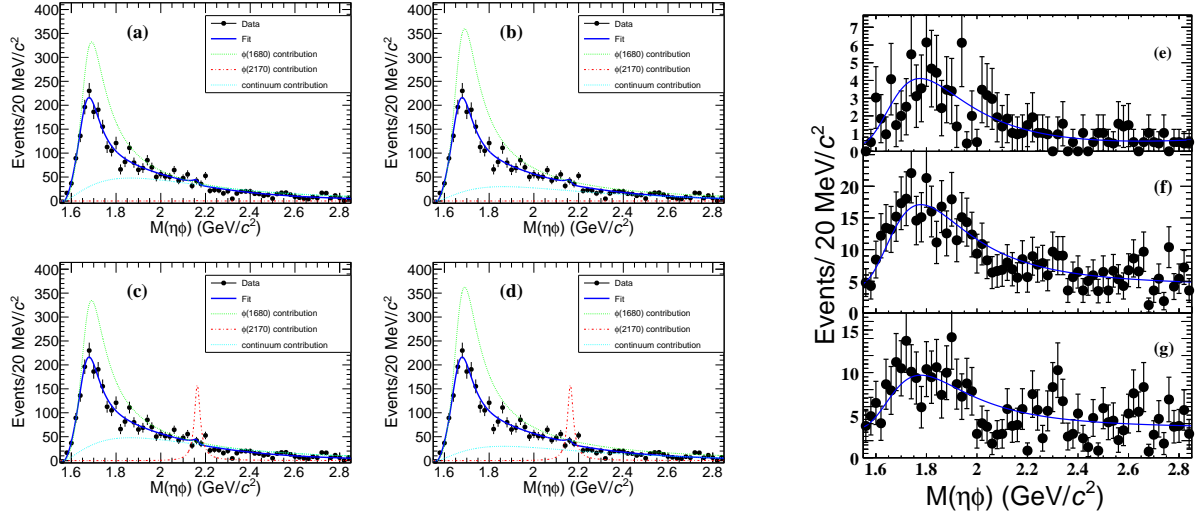


FIG. 4. Invariant mass distribution of  $M(\eta\phi)$ , and fit results. (a-d) show the four solutions, and (e-g) show the backgrounds estimated from 2D sidebands. In (a-d), the backgrounds estimated from 2D sidebands have been subtracted. The distribution in (e) shows events from the sideband region  $S_3$ , (f) from  $S_2$  and (g) from  $S_1$ , respectively. The curves show the best fit results, while the interference among continuum,  $\phi(1680)$  and  $\phi(2170)$  are not shown.

TABLE I. Fit results with  $\phi(1680)$  and  $\phi(2170)$  both included, and also excluding  $\phi(2170)$ . The mass and width of  $\phi(2170)$  are fixed from the prior BESIII measurement [25].

Parameters	with $\phi(2170)$				without $\phi(2170)$	
	Solution I	Solution II	Solution III	Solution IV	Solution I	Solution II
$\chi^2/ndf$	77/56				85/60	
$a_0$	$-4.1 \pm 0.5$	$5.0 \pm 0.7$	$-5.0 \pm 0.5$	$-4.8 \pm 0.2$	$-3.2 \pm 0.7$	$5.0 \pm 0.1$
$a_1$	$2.7 \pm 0.1$	$2.6 \pm 0.1$	$2.7 \pm 0.1$	$2.6 \pm 0.1$	$2.9 \pm 0.1$	$2.6 \pm 0.1$
$\mathcal{B}_{\eta\phi}^{\phi(1680)} \Gamma_{e^+e^-}^{\phi(1680)} (\text{eV})$	$122 \pm 6$	$219 \pm 15$	$163 \pm 11$	$203 \pm 12$	$75 \pm 10$	$207 \pm 16$
$M_{\phi(1680)} (\text{MeV}/c^2)$	$1683 \pm 7$				$1696 \pm 8$	
$\Gamma_{\phi(1680)} (\text{MeV})$	$149 \pm 12$				$175 \pm 13$	
$\mathcal{B}_{\eta\phi}^{\phi(1680)}$	$0.18 \pm 0.02$	$0.19 \pm 0.04$	$0.21 \pm 0.02$	$0.17 \pm 0.04$	$0.25 \pm 0.12$	$0.23 \pm 0.10$
$\mathcal{B}_{\eta\phi}^{\phi(2170)} \Gamma_{e^+e^-}^{\phi(2170)} (\text{eV})$	$0.09 \pm 0.05$	$0.06 \pm 0.02$	$16.7 \pm 1.2$	$17.0 \pm 1.2$	—	
$M_{\phi(2170)} (\text{MeV}/c^2)$	$2163.5(\text{fixed})$				—	
$\Gamma_{\phi(2170)} (\text{MeV})$	$31.1(\text{fixed})$				—	
$\theta_{\phi(1680)} (^\circ)$	$-89 \pm 2$	$96 \pm 6$	$-92 \pm 1$	$-86 \pm 7$	$-87 \pm 15$	$108 \pm 22$
$\theta_{\phi(2170)} (^\circ)$	$37 \pm 14$	$-102 \pm 11$	$-167 \pm 6$	$-155 \pm 5$	—	



## V. CROSS SECTION FOR $e^+e^- \rightarrow \eta\phi$

The  $M_{\eta\phi}$  distributions in Fig. 3 are combined and the cross section of  $e^+e^- \rightarrow \eta\phi$  for each  $M_{\eta\phi}$  bin is calculated according to

$$\sigma_i = \frac{n_i^{\text{obs}} - n_i^{\text{bkg}}}{\mathcal{L}_i \times \sum_j \varepsilon_{ij} \mathcal{B}_j}, \quad (7)$$

where  $i$  is the  $i$ -th bin of the combined  $M_{\eta\phi}$  distribution and  $j$  is the  $j$ -th  $\eta$  decay mode;  $n_i^{\text{obs}}$ ,  $n_i^{\text{bkg}}$ ,  $\varepsilon_{ij}$ ,  $\mathcal{L}_i$ , and  $\mathcal{B}_j$  are the number of events observed in data, the number of background events estimated from the 2D sidebands, the efficiency of signal selection, the effective integrated luminosity of ISR production in Belle data, and the branching fractions of  $\eta$  and  $\phi$  decays [32], respectively. The cross sections for  $e^+e^- \rightarrow \eta\phi$  measured with Belle data are shown in Fig. 5, where the error bars include the statistical uncertainties and the systematic uncertainties in the background estimation using the 2D sidebands. A 6.7% common uncertainty (described in Sec. VI and Table II) is not shown in Fig. 5. The cross sections for  $e^+e^- \rightarrow \eta\phi$  are around 2.6 nb and 0.4 nb at the  $\phi(1680)$  and  $\phi(2170)$  peaks, respectively. The measured cross section is in good agreement with the results from BaBar's measurement [22], but with improved precision.

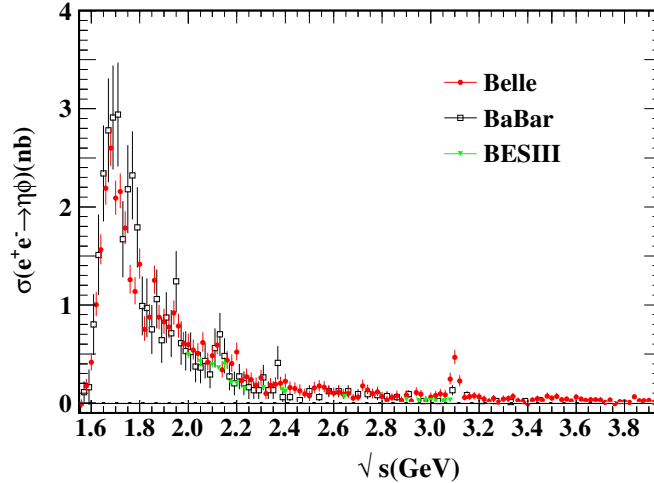


FIG. 5. Cross section for  $e^+e^- \rightarrow \eta\phi$  from threshold to 3.95 GeV. The errors are the combination of statistical errors and the systematic uncertainties due to the 2D sideband subtraction. A systematic uncertainty of 6.7% common to all the data points is not shown.

## VI. SYSTEMATIC UNCERTAINTIES

The following systematic uncertainties are characterized for this analysis. The uncertainties due to the particle identification are 2.0% in the  $\gamma\gamma$  mode and 4.0% in  $\pi^+\pi^-\pi^0$ , respectively. The uncertainty due to the tracking efficiency is 0.35% per track and is additive; the uncertainty in the photon reconstruction is 2% per photon. The uncertainties in

the  $\phi$  mass,  $\eta$  mass, and  $M_{\text{miss}}^2(\gamma_{\text{ISR}}\eta\phi)$  requirements are measured with the control sample  $e^+e^- \rightarrow J/\psi \rightarrow \eta\phi$ ; 1.3% for the  $\eta$  mass window is taken as a conservative uncertainty for the combined  $\pi^+\pi^-\pi^0$  and  $\gamma\gamma$  modes. For the  $\phi$  mass window, the corresponding value is 0.5%. Similarly, 1.3% is taken to be a conservative systematic uncertainty estimate, due to the  $M_{\text{miss}}^2(\gamma_{\text{ISR}}\eta\phi)$  requirement.

Belle measures luminosity with 1.4% precision while the uncertainty of the generator PHOKHARA is less than 1% [29]. The trigger efficiencies for the events surviving the selection criteria are  $(97.0 \pm 0.1)\%$  for the  $\pi^+\pi^-\pi^0$  mode and  $(95.1 \pm 0.1)\%$  for the  $\gamma\gamma$  mode according to the trigger simulation. Conservative uncertainties of 1.0% and 1.5% are taken to be the systematic uncertainties in the trigger efficiencies for the  $\pi^+\pi^-\pi^0$  mode and  $\gamma\gamma$  modes [8, 34]. The uncertainties in the  $\phi$  and  $\eta$  branching fractions are calculated according to the world average values [32], which contribute a systematic uncertainty of 0.6%. The statistical uncertainty in the MC determination of the efficiency is 0.1%.

Assuming all these sources are independent and adding them in quadrature, the total systematic uncertainties in measuring  $\mathcal{B}(J/\psi \rightarrow \eta\phi)$  are 7.9% for the  $\pi^+\pi^-\pi^0$  mode and 7.2% for the  $\gamma\gamma$  mode. There are some common uncertainties related to detection efficiency in the two modes, as listed in Table II. For other uncertainties that have no correlation between two modes, these are first summed in quadrature to obtain  $\sigma_i$ . Then the total independent uncertainty ( $\sigma_{\text{tot}}$ ) is calculated by  $\sqrt{\sum_i (\Delta\varepsilon_i \times \mathcal{B}_i)^2 / \sum_i (\varepsilon_i \times \mathcal{B}_i)}$ , where  $\Delta\varepsilon_i$  equal to  $\sigma_i \times \varepsilon_i$ ,  $i$  is  $i$ th mode of  $\eta$  decays ( $i = \pi^+\pi^-\pi^0, \gamma\gamma$ ). The value of  $\sigma_{\text{sys}}$  is calculated by  $\sqrt{\sum_j (\sigma_j)^2 + (\sigma_{\text{tot}})^2}$  ( $\sigma_j$  designates each common uncertainty mentioned above), and the total systematic uncertainty in the cross section measurement thereby calculated to be 6.8%.

By changing the fit range to [1.6, 2.9] GeV/ $c^2$ , the systematic uncertainty due to the fit range is found to be negligible. To estimate the model dependence of the non-resonant contribution, we use  $A_{\eta\phi}^{n.r.}(s) = a_0/s$ . The uncertainties in backgrounds from the 2D sidebands are estimated by changing  $a$  or  $b$  by  $1\sigma$ , and changing the functions used to parameterize them, as mentioned in Sec. IV. Systematic uncertainties in the cross section resulting from different sideband background parameterizations are also shown in Fig. 5; these translate to uncertainties in the number of  $J/\psi$  signal events of 1.8% in the  $\gamma\gamma$  mode and 1.5% in the  $\pi^+\pi^-\pi^0$  mode. The uncertainty in  $\mathcal{B}_{\phi(1680)}^{KK^*(892)} / \mathcal{B}_{\phi(1680)}^{\eta\phi}$  is obtained by varying  $1\sigma$  according to the previous measurement [22].

## VII. SUMMARY

In summary, the  $e^+e^- \rightarrow \eta\phi$  cross sections are measured from threshold to 3.95 GeV. The branching fraction of  $J/\psi \rightarrow \eta\phi$  is measured to be  $(7.1 \pm 1.0 \pm 0.5) \times 10^{-4}$ , which is in good agreement with the world average value [32]. There are four solutions with the same fit quality but different phase angles, obtained from fitting the invariant mass distributions of  $\eta\phi$  and including both  $\phi(1680)$  and  $\phi(2170)$ . The resonant parameters of  $\phi(1680)$  are obtained to be  $M_{\phi(1680)} = (1683 \pm 7 \pm 9) \text{ MeV}/c^2$ ,  $\Gamma_{\phi(1680)} = (149 \pm 12 \pm 13) \text{ MeV}$ , and  $\mathcal{B}_{\phi(1680)}^{\eta\phi} \Gamma_{\phi(1680)}^{e^+e^-} = (122 \pm 6 \pm 13) \text{ eV}$ ,  $(219 \pm 15 \pm 18) \text{ eV}$ ,  $(163 \pm 11 \pm 13) \text{ eV}$  or  $(203 \pm 12 \pm 18) \text{ eV}$  for the four solutions. The branching fraction for  $\phi(1680) \rightarrow \eta\phi$  is determined to be  $(18 \pm 2 \pm 1)\%$ ,  $(19 \pm 4 \pm 2)\%$ ,  $(21 \pm 2 \pm 1)\%$  or  $(17 \pm 4 \pm 2)\%$  for the four solutions. We do not find a significant  $\phi(2170)$  signal in the Belle data, and instead set an upper limit on its production of  $\mathcal{B}_{\phi(2170)}^{\eta\phi} \Gamma_{\phi(2170)}^{e^+e^-} < 0.17 \text{ eV}$  or  $< 18.6 \text{ eV}$  at 90% C.L.; both are consistent the BESIII

TABLE II. Summary of systematic uncertainties (%) for the measurements of  $\mathcal{B}(J/\psi \rightarrow \eta\phi)$  and  $\sigma(e^+e^- \rightarrow \eta\phi)$ . Fit uncertainties already described in the text are not included here.

Source	$\gamma\gamma$ mode	$\pi^+\pi^-\pi^0$ mode	common
Particle identification	2.0	4.0	2.0
Tracking	0.7	1.4	0.7
Photon reconstruction	6.0	6.0	6.0
$\phi$ , $\eta$ masses and $M_{\text{miss}}^2(\eta\phi\gamma_{\text{ISR}})$	1.7	1.4	1.4
Luminosity	1.4	1.4	1.4
Generator	0.5	0.5	0.5
$\sigma_{\text{ISR}}^{\text{prod}}(J/\psi)$	1.0	1.0	1.0
Trigger	1.5	1.0	...
Branching fractions	0.6	0.6	0.6
$J/\psi$ signal fitting	1.8	1.5	...
MC statistics	0.1	0.1	0.1
Sum for $\sigma(e^+e^- \rightarrow \eta\phi)$	6.9	7.3	6.7
Sum for $\mathcal{B}(J/\psi \rightarrow \eta\phi)$	7.2	7.9	6.8

measurement [25].

## ACKNOWLEDGMENTS

We thank the KEKB group for the excellent operation of the accelerator; the KEK cryogenics group for the efficient operation of the solenoid;

- 
- [1] For a recent review, see S. L. Olsen, T. Skwarnichi and D. Zieminska, Rev. Mod. Phys., **90**, 015003 (2018).
  - [2] S. Choi *et al.* (Belle Collaboration), Phys. Rev. Lett. **91**, 262001 (2003).
  - [3] M. Ablikim *et al.* (BESIII Collaboration), Phys. Rev. Lett. **110**, 252001 (2013); Liu *et al.* (Belle Collaboration), Phys. Rev. Lett. **110**, 252002 (2013).
  - [4] M. Ablikim *et al.* (BESIII Collaboration), Phys. Rev. Lett. **111**, 242001 (2013).
  - [5] X. L. Wang *et al.* (Belle Collaboration), Phys. Rev. D **91**, 112007 (2015); M. Ablikim *et al.* (BESIII Collaboration), Phys. Rev. D **96**, 032004 (2017).
  - [6] B. Aubert *et al.* (BaBar Collaboration), Phys. Rev. Lett. **95**, 142001 (2005).
  - [7] B. Aubert *et al.* (BaBar Collaboration), Phys. Rev. D **74**, 091103 (2006).
  - [8] C. P. Shen *et al.* (Belle Collaboration), Phys. Rev. D **80**, 031101 (2009).
  - [9] G. J. Ding and M. L. Yan, Phys. Lett. B **657**, 49 (2007); Q. Li *et al.* arXiv: 2004.05786.
  - [10] T. Barnes, N. Black and P. R. Page, Phys. Rev. D **68**, 054014 (2003).
  - [11] G. J. Ding and M. L. Yan, Phys. Lett. B **650**, 390 (2007).
  - [12] P. R. Page, E. S. Swanson and A. P. Szczepaniak Phys. Rev. D **59**, 034016 (1999).
  - [13] Z. G. Wang, Nucl. Phys. A **791**, 106 (2007).
  - [14] H. X. Chen, X. Liu, A. Hosaka and S. L. Zhu, Phys. Rev. D **78**, 034012 (2008).

- [15] E. Klemp and A. Zaitsev, Phys. Rep. **454**, 1 (2007).
- [16] C. F. Qiao, Phys. Lett. B **639**, 263 (2006).
- [17] Y. Dong, A. Faessler, T. Gutsche, Q. Lu, and V. E. Lyubovitskij, Phys. Rev. D **96**, 074027 (2017).
- [18] Y. L. Yang, D. Y. Chen and Z. Lu Phys. Rev. D **100**, 073007 (2019).
- [19] S. L. Zhu, Int. J. Mod. Phys. A **E17**, 283 (2008).
- [20] A. M. Torres, K. P. Khemchandani, L. S. Geng, M. Napsuciale and E. Oset, Phys. Rev. D **78**, 074031 (2008).
- [21] Y. H. Ma, Y. Chen, M. Gong and Z. F. Liu, arXiv:2007.14893v1.
- [22] B. Aubert *et al.* (BaBar Collaboration), Phys. Rev. D **76**, 092005 (2007); B. Aubert *et al.* (BaBar Collaboration), Phys. Rev. D **77**, 092002 (2008).
- [23] V. L. Ivanov *et al.*, Phys. Lett. B **798**, 134946 (2019).
- [24] M. Ablikim *et al.* (BESIII Collaboration), Phys. Rev. D **102**, 012008 (2020).
- [25] M. Ablikim *et al.* (BESIII Collaboration), Phys. Rev. D **104**, 032007 (2021).
- [26] A. Abashian *et al.* (Belle Collaboration), Nucl. Instrum. Methods Phys. Res. Sect. A **479**, 117 (2002); also see detector section in J. Brodzicka *et al.*, Prog. Theor. Exp. Phys. **2012**, 04D001 (2012).
- [27] S. Kurokawa and E. Kikutani, Nucl. Instrum. Methods Phys. Res. Sect. A **499**, 1 (2003), and other papers included in this Volume; T. Abe *et al.*, Prog. Theor. Exp. Phys. **2013**, 03A001 (2013) and references therein.
- [28] A. Keshavarzi, D. Nomura and T. Teubner, Phys. Rev. D **97**, 114025 (2018).
- [29] G. Rodrigo *et al.*, Eur. Phys. J. C **24**, 71 (2002). For a review on the generator, see: S. Actis *et al.*, Eur. Phys. J. C **66**, 585 (2010).
- [30] R. Brun *et al.*, GEANT 3.21, CERN DD/EE/84-1, 1984.
- [31] E. Nakano, Nucl. Instrum. Methods A **494**, 402 (2002).
- [32] P. A. Zyla *et al.* (Particle Data Group), Prog. Theor. Exp. Phys. **2020**, 083C01(2020) and 2021 update.
- [33] E. A. Kuraev and V. S. Fadin, Sov. J. Nucl. Phys. **41**, 466 (1985) [Yad. Fiz. **41**, 733 (1985)].
- [34] X. L. Wang *et al.* (Belle Collaboration), Phys. Rev. D **87**, 051101 (2013).